UC San Diego
UC San Diego Previously Published Works

Title

Performance of polarization diversity in correlated Nakagami-m fading channels

Permalink

https://escholarship.org/uc/item/7402q7j3

Journal

IEEE Transactions on Vehicular Technology, 55(1)

ISSN

0018-9545

Authors

Jootar, J

Diouris, J F

Zeidler, J R

Publication Date

2006

Peer reviewed

Performance of Polarization Diversity in Correlated Nakagami-m Fading Channels

Jittra Jootar, *Student Member, IEEE*, Jean-Francois Diouris, *Member, IEEE*, and James R. Zeidler, *Fellow, IEEE*

Abstract—This paper analyzes the performance of systems with dual-polarized antennas in correlated Nakagami-m fading channels as a function of envelope correlation and cross-polarization discrimination by means of the characteristic function of the instantaneous post-maximal ratio combining (MRC) signal-to-noise ratio (SNR). Systems of interest include systems with receive polarization diversity and systems with transmit and receive polarization diversity employing Alamouti space-time code. The expressions for the average symbol error probability as a function of SNR assuming no power control, and the expressions for the average required transmit power to achieve the constant desired post-MRC SNR assuming perfect fast power control, are derived. Finally, a comparison between analytical and simulation results is used to validate the analysis.

Index Terms—Fading, maximal radio combining (MRC), polarization diversity, power control, transmit diversity.

I. INTRODUCTION

IT IS well known that increasing the number of antennas in a wireless communication system can effectively improve the system performance. However, the cost of increasing the spatial dimensions at the base station and the handsets has been an impediment to the deployment of spatial diversity in practical systems. Polarization diversity provides an alternative means of increasing the diversity order with little increase in the spatial dimensions. The diversity is produced by the depolarization of the transmitted signal by reflection, diffraction, and scattering in the channel [1], [2]. Without polarization receive diversity, the signal energy residing in the polarization orthogonal to the polarization of the receive antenna cannot be utilized. Another advantage of polarization diversity is the ability to recover from a polarization mismatch, which occurs when the polarization of the transmit antenna and the receive antenna are different. In wireless communication systems where antennas at the mobile units are randomly oriented, polarization receive diversity collects signal energy from multiple polarizations, allowing improved performance in a spatially compact array [3].

J. Jootar and J. R. Zeidler are with the Department of Electrical and Computer Engineering, University of California at San Diego, La Jolla, CA 92093-0407 USA (e-mail: jjootar@ucsd.edu; zeidler@ece.ucsd.edu).

J.-F. Diouris is with Institut de Recherche en Communication et Cyberné tique de Nates, Ecole Polytechnique de l'université de Nantes, BP 50609, 44306 Nantes Cedex 03, France (e-mail: jean-francois.diouris@polytech.univ-nantes.fr).

One limitation of polarization diversity is an intrinsic power imbalance. The nature of electromagnetic wave propagation dictates that the polarization orthogonal to the obstacle is attenuated more than the polarization parallel to the obstacle [1], [2]. Considering that buildings are typical obstacles in wireless channels, the horizontal polarization (HPol) is expected to be attenuated more that the vertical polarization (VPol). This asymmetrical attenuation can lead to a significant power imbalance, which will further degrade the system performance [1], [2], [4], [5].

The characteristics of polarization diversity have been described by envelope correlation (ρ_{env}) and cross-polarization discrimination (XPD or χ). The envelope correlation represents the correlation between the polarizations. The XPD represents the power imbalance between the polarizations and is defined as the ratio between the copolarized signal power and the cross-polarized signal power. Given that the transmitted signal is vertically polarized, the XPD is the ratio between the average signal power received from the VPol and the average signal power received from the HPol. These parameters strongly depend on the specific channel characteristics, and extensive field measurements have been conducted to determine realistic values of ρ_{env} and χ. Experimental data have shown that the envelope correlation between the VPol and the HPol at the receiver is generally less than 0.2 [2]–[6]. Furthermore, the XPD in the urban environment, given that a vertically polarized signal is transmitted, is normally between 1 and 10 dB, with an average of 6 dB [2], [4], [5]. The XPD in the rural environment is usually more than 10 dB [2] due to the lack of obstacles that couple the signal from the VPol into the HPol. The values of ρ_{env} and XPD measured from urban environments will be used as an example of realistic channel characteristics. Note that this system model may not represent some practical implementations, such as the uplink of cellular systems, where the transmit antenna is not vertically oriented, or a system with cross-polarization antennas, which consists of $\pm 45°$ slanted antennas. However, performance gain of these systems can be obtained by replacing ρ_{env} and χ used in this analysis with those of the system under interest.

Previous results which quantify various aspects of the performance gains of polarization diversity are discussed in [1]–[4] and [11]. In [2], the gain is defined as the increase in the measured combined signal power from the VPol and the HPol, compared to the VPol only, corresponding to a certain percentile of the power. Lotse *et al.* used simulations based on the XPD and the envelope correlation measurement to find the performance gain [4]. Turkmani *et al.* used measured fading coefficients to find the gain as a function of XPD and envelope correlation for selection, equal gain, and maximal ratio combining techniques

and used curve fitting to produce expressions for the polarization diversity gain at 90% signal reliability [3]. Visoz and Bejjani derived an analytical expression for the matched filter bound error probability for the binary phase-shift keying (BPSK) modulation in correlated Rayleigh fading channels assuming no power control [1]. Nabar *et al.* used the Chernoff bound to derive the performance gain for transmit and receive polarization diversity using Alamouti space-time code [11]. The goal of this paper is to analytically derive the performance of polarization diversity systems as a function of the measured channel characteristic in a more general form by using the characteristic function of the instantaneous SNR at the receiver. Although this paper focuses on polarization diversity, the same analytical approach can also be applied to other correlated fading systems with unequal average receive signal power between diversity branches.

In this paper, we extend the study presented in [7], which derived the performance of polarization receive diversity systems in correlated Rayleigh fading channels, where maximal ratio combining (MRC) is used at the receiver, to correlated Nakagami-m fading channels [8]. The characteristic function of the instantaneous SNR at the output of the MRC suggested in [9] is used to derive the system performance as a function of ρ_{env} and χ. Systems studied in this paper include systems with polarization receive diversity, and systems with both polarization transmit diversity and polarization receive diversity employing Alamouti space-time code [10]. Two types of power control assumptions are investigated, namely, no power control and perfect fast power control. We derive expressions for the average symbol error probability as a function of SNR assuming no power control. For the perfect fast power control assumption, we derive expressions for the average transmit power required to achieve the constant desired post-MRC SNR. To appreciate the simplicity and flexibility of this approach, we extend the result of the system with Alamouti space-time code, assuming no power control to 16-QAM, and compare our analytical results to the results derived from the Chernoff bound approach [11] and our simulation results.

The paper is organized as follows. Section II describes the system model. Section III discusses the system performance assuming no power control or perfect fast power control. Section IV discusses the analytical results. Finally, the conclusion is presented in Section V.

II. SYSTEM MODEL

Although the analysis can be applied to any number of antennas, this paper focuses on three practical systems. Two types of antenna configurations are used in these systems, namely, the single-polarized antenna, which consists of a VPol antenna, and the dual-polarized antenna, which consists of collocated VPol and HPol antennas. The systems of interest are the following.
1) *System A: One Vpol transmit antenna and one dual-polarized receive antenna.* This system can be viewed as a supoptimal two-branch receive diversity system. When the space constraint prevents spatial diversity from being deployed, diversity is added to the system via polarization diversity.
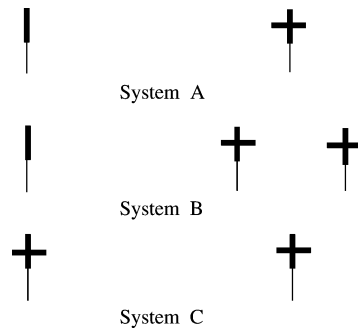

Fig. 1. Illustrations of system A, B, and C.

2) *System B: One Vpol transmit antenna and two dual-polarized receive antennas.* System B is the system in which the space constraint allows two spatially separated VPol antennas to be deployed. Instead of using two VPol receive antennas, the system performance can be improved by adding an HPol antenna to each of the existing VPol antennas, making this system a spatial and polarization receive diversity system.
3) *System C: One dual-polarized transmit antenna and one dual-polarized receive antenna.* This system is an improvement from system A because of the added space-time code, which utilizes transmit diversity from the dual-polarized antenna at the transmitter.

Fig. 1 shows illustrations of systems A, B, and C. Note that antennas on the left are transmit antennas, and antennas on the right are receive antennas.

The channel is assumed to be a multilink channel, where the transmitted signal is received over M slowly-varying flat fading channels. The envelope of the complex fading coefficient is assumed to be Nakagami-m distributed with the dominant branch having a unit average power [8]. The phase of the complex fading coefficient is assumed to be uniformly distributed ranging from 0 to 2π. The signals received from collocated antennas are assumed to be correlated, while the signals received from spatially separated antennas are assumed to be uncorrelated. The transmitter and the receiver are assumed to have perfect knowledge of the channel state information. At the receiver, MRC is used to combine the received signals.

A. System A and System B

The baseband equivalent of the signal received at the kth receive antenna of the system with M receive antennas is

$$x_k = \sqrt{E_b}\,\alpha_k s + n_k \tag{1}$$

where E_b is the transmit energy per bit; α_k is the complex fading coefficient at the kth antenna; s is the data symbol, ± 1 for BPSK, $\pm 1 \pm j$ for quadrature phase-shift keying (QPSK); and n_k is the noise at the kth antenna.

Note that n_k is the baseband equivalent of the AWGN noise, i.e., a circularly symmetric, zero-mean Gaussian random process with $E[n_k n_k^*] = 2\sigma^2 = \eta_o$. Noise components from different receiver branches are assumed to be independent and identically distributed.

Signals received from multiple antennas are combined using the MRC diversity receiver. The received signal, multiplied by the conjugate of the channel estimate, can be expressed as

$$y_k = \sqrt{E_b}|\alpha_k|^2 s + \alpha_k^* n_k \qquad (2)$$

where α^* denotes the complex conjugate of α.

The post-MRC SNR per bit (φ) can be expressed as

$$\varphi = \sum_{k=1}^{M} \frac{E_b|\alpha_k|^2}{\eta_o} = E_b \gamma$$

$$\text{where } \gamma = \sum_{k=1}^{M} \frac{|\alpha_k|^2}{\eta_o} \qquad (3)$$

The characteristic function of γ for an M-branch MRC diversity receiver in Nakagami-m distribution channels [9] is

$$\Phi_\gamma(s) = \left| I_M - js\frac{\bar{\gamma}}{m}\Lambda \right|^{-m} \qquad (4)$$

where I_M is an M-by-M identity matrix; $\bar{\gamma}$ is the mean of γ; m is the Nakagami-m distribution parameter, where the channels with $m = (1/2), 1$, and ∞ corresponds to the one-sided Gaussian channel, the Rayleigh channel, and the AWGN channel, respectively; Λ is an M-by-M correlation matrix; and $|A|$ is the determinant of matrix A.

The correlation matrix Λ, described in [9], can be summarized as follows:

$$\Lambda_{kl} E[a_k a_k] = E[a_k a_l] + jE[a_k b_l] = \Lambda_{lk}^* E[a_l a_l] \quad (5a)$$

$$E[a_k a_k] = E[a_l a_l] \qquad (5b)$$

$$E[a_k b_l] = -E[a_l b_k] \qquad (5c)$$

where $\alpha_k = a_k + jb_k$, and Λ_{kl} is the element corresponding to the kth row and the lth column of Λ.

Because of the power imbalance of polarization diversity systems, the equal average power assumption in [9] is invalid; therefore, some modifications are necessary in order to proceed with the analysis. First, we assume that the system has N dual-polarized receive antennas, where V_k and H_k represent the VPol antenna and the HPol antenna of the kth dual-polarized antenna, respectively. Second, we assume equal average receive signal power on all VPol antennas, equal average receive signal power on all HPol antennas, and the ratio between the average receive signal power of VPol antennas and the average receive signal power of HPol antennas is χ. Using the vertical branches as the reference branch, elements in the new correlation matrix can be described as

$$\Lambda_{V_k V_k} = \chi \Lambda_{H_k H_k} = 1, \quad \text{for } 1 \geq k \geq N \qquad (6a)$$

$$\Lambda_{V_l H_k} = 0 \quad \text{when } l \neq k \qquad (6b)$$

$$\Lambda_{V_k H_k} \approx \sqrt{\frac{\rho_{\text{env}}}{\chi}}. \qquad (6c)$$

Note that the approximation in (6c) is from the observation that the correlation coefficient of the two polarization components in Rayleigh fading channels can be approximated as the square
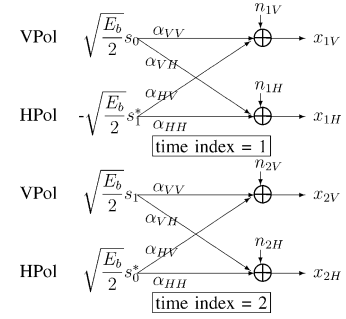

Fig. 2.   Block diagram for system C.

root of the envelope correlation [12]. Due to lack of experimental result on polarization characteristics of Nakagami-m fading channels, we will assume that this approximation is valid for Nakagami-m fading channels as well.

Using the results from (6a)–(6c), the correlation matrix for system A and system B can be obtained as

$$\Lambda_A = \begin{bmatrix} 1 & \sqrt{\dfrac{\rho_{\text{env}}}{\chi}} \\ \sqrt{\dfrac{\rho_{\text{env}}}{\chi}} & \dfrac{1}{\chi} \end{bmatrix} \qquad (7)$$

$$\Lambda_B = \begin{bmatrix} 1 & \sqrt{\dfrac{\rho_{\text{env}}}{\chi}} & 0 & 0 \\ \sqrt{\dfrac{\rho_{\text{env}}}{\chi}} & \dfrac{1}{\chi} & 0 & 0 \\ 0 & 0 & 1 & \sqrt{\dfrac{\rho_{\text{env}}}{\chi}} \\ 0 & 0 & \sqrt{\dfrac{\rho_{\text{env}}}{\chi}} & \dfrac{1}{\chi} \end{bmatrix}. \qquad (8)$$

Notice that with $0 \leq \rho_{\text{env}} \leq 1$ and $\chi \geq 1$, both Λ_A and Λ_B are positive semi-definite.

B. System C

In addition to the assumptions made for system A and system B, the analysis for system C also assumes that the channel changes slowly, such that the fading coefficients between two consecutive symbols are the same. For consistency, the transmit power for system C refers to the total transmit power, which is equal to twice the power transmitted from each antenna. Fig. 2 shows the signal sequence and the fading coefficients of system C. The signals at each of the receive antenna can be expressed as

$$x_{1V} = \sqrt{\frac{E_b}{2}}(\alpha_{VV} s_0 - \alpha_{HV} s_1^*) + n_{1V} \qquad (9a)$$

$$x_{1H} = \sqrt{\frac{E_b}{2}}(\alpha_{VH} s_0 - \alpha_{HH} s_1^*) + n_{1H} \qquad (9b)$$

$$x_{2V} = \sqrt{\frac{E_b}{2}}(\alpha_{VV} s_1 + \alpha_{HV} s_0^*) + n_{2V} \qquad (9c)$$

$$x_{2H} = \sqrt{\frac{E_b}{2}}(\alpha_{VH} s_1 + \alpha_{HH} s_0^*) + n_{2H}. \qquad (9d)$$

Because of the orthogonality between the sequences transmitted from the VPol antenna and the HPol antenna, the original

symbol can be recovered completely. The signals after MRC becomes

$$y_1 = s_1 \sqrt{\frac{E_b}{2}} (|\alpha_{VV}|^2 + |\alpha_{VH}|^2 + |\alpha_{HV}|^2 + |\alpha_{HH}|^2) + \tilde{n}_1$$

(10a)

$$y_2 = s_2 \sqrt{\frac{E_b}{2}} (|\alpha_{VV}|^2 + |\alpha_{VH}|^2 + |\alpha_{HV}|^2 + |\alpha_{HH}|^2) + \tilde{n}_2$$

(10b)

where $\tilde{n}_1$ and $\tilde{n}_2$ represent the noise after combining, and $E[|\tilde{n}_1|^2] = E[|\tilde{n}_2|^2] = 2\sigma^2 (|\alpha_{VV}|^2 + |\alpha_{VH}|^2 + |\alpha_{HV}|^2 + |\alpha_{HH}|^2)$.

The post-MRC SNR is

$$\varphi_C = \frac{E_b}{2\eta_o} (|\alpha_{VV}|^2 + |\alpha_{VH}|^2 + |\alpha_{HV}|^2 + |\alpha_{HH}|^2) = \frac{E_b \gamma}{2}.$$

(11)

The characteristic function of γ can also be represented with the characteristic function shown in (4). The correlation matrix for system C can be written as

$$\Lambda_C = \begin{bmatrix} 1 & \sqrt{\frac{t_1}{\chi_1}} & \sqrt{\frac{\delta r_1}{\chi_2}} & 0 \\ \sqrt{\frac{t_1}{\chi_1}} & \frac{1}{\chi_1} & 0 & \sqrt{\frac{\delta r_2}{\chi_1}} \\ \sqrt{\frac{\delta r_1}{\chi_2}} & 0 & \frac{\delta}{\chi_2} & \delta\sqrt{\frac{t_2}{\chi_2}} \\ 0 & \sqrt{\frac{\delta r_2}{\chi_1}} & \delta\sqrt{\frac{t_2}{\chi_2}} & \delta \end{bmatrix}$$

(12)

where t_1, t_2, r_1, and r_2 are the envelope correlation between $\{\alpha_{VV}$ and $\alpha_{VH}\}$, $\{\alpha_{HV} \alpha_{HH}\}$, $\{\alpha_{VV}$ and $\alpha_{HV}\}$, and $\{\alpha_{VH}$ and $\alpha_{HH}\}$, respectively. χ_1 is the ratio between the signal power received from the VPol receive antenna and the signal power received from the HPol receive antenna, given that the VPol signal is transmitted. χ_2 is the ratio between the signal power received from the HPol receive antenna and the signal power received from the VPol receive antenna, given that the HPol signal is transmitted. δ is the ratio between the signal power received from the HPol antenna, given the HPol signal is transmitted and the signal power received from the VPol antenna, given the VPol signal, is transmitted.

Experimental data have shown that the correlation between fading coefficients that originate from different transmit antennas and arrive at different antennas ($\{\alpha_{VV}$ and $\alpha_{HH}\}$ or $\{\alpha_{VH}$ and $\alpha_{HV}\}$) are very small [6]. With the assumption that these values are negligible, we can approximate the anti-diagonal elements of Λ_C to be zero.

Note that with $0 \leq t_1, t_2, r_1, r_2 \leq 1$, and $\chi_1, \chi_2 \geq 1$, Λ_C is positive semi-definite.

III. PERFORMANCE ANALYSIS

This paper focuses on two power control scenarios: no power control and perfect fast power control.

A. No Power Control

The signal power in this mode does not change with time. The performance is measured by the average symbol error probability corresponding to the SNR. From [9], the average symbol error probability of a coherent BPSK system is given by

$$\bar{P}_e = \frac{1}{\pi} \int_0^{\frac{\pi}{2}} \left| I_M + \frac{\bar{\varphi}}{m \sin^2 \nu} \Lambda \right|^{-m} d\nu$$

(13)

where I_M, m, and Λ are as previously defined, and $\bar{\varphi}$ is the expectation of φ and is equal to $E_b \bar{\gamma}$ for system A, B and is equal to $E_b \bar{\gamma}/2$ for system C.

Since the symbol error which dominates the system performance at high SNR is the error between the transmitted symbol and its nearest neighbors, the average symbol error can be approximated by considering only the nearest neighbor error events [13]

$$\bar{P}_e \approx \sum_{i=1}^{N_{\text{sym}}} Pr(S_i) N_e(S_i) Q\left(\frac{d_{\min}(S_i)}{2\sigma}\right)$$

(14)

where N_{sym} is the number of symbols in the constellation, $Pr(S_i)$ is the probability of the symbol S_i being transmitted, $N_e(S_i)$ is the number of the nearest neighbors of symbol S_i, $d_{\min}(S_i)$ is the minimum distance to the nearest neighbors of symbol S_i, and σ_n^2 is the noise variance [13]. Therefore, the average symbol error probability of a coherent QPSK system, assuming equally likely transmit symbols, can be approximated as

$$\bar{P}_e \approx \frac{2}{\pi} \int_0^{\frac{\pi}{2}} \left| I_M + \frac{\bar{\varphi}}{m \sin^2 \nu} \Lambda \right|^{-m} d\nu.$$

(15)

The symbol error probability of systems A, B, and C can be found by substituting Λ with the correlation matrix shown in (7), (8), and (12). The expressions for the average symbol error probability can be simplified as

$$\bar{P}_{e,A} \approx \frac{\bar{N}_e}{\pi} \int_0^{\frac{\pi}{2}} \left(1 + \frac{\bar{\varphi}\xi}{m \sin^2 \nu} - \frac{\bar{\varphi}^2 \delta}{m^2 \sin^4 \nu}\right)^{-m} d\nu$$

(16a)

$$\bar{P}_{e,B} \approx \frac{\bar{N}_e}{\pi} \int_0^{\frac{\pi}{2}} \left(1 + \frac{\bar{\varphi}\xi}{m \sin^2 \nu} - \frac{\bar{\varphi}^2 \delta}{m^2 \sin^4 \nu}\right)^{-2m} d\nu$$

(16b)

$$\bar{P}_{e,C} \approx \frac{\bar{N}_e}{\pi} \int_0^{\frac{\pi}{2}} \prod_{i=1}^{4} \left(1 + \frac{\bar{\varphi}\lambda_i}{2m \sin^2 \nu}\right)^{-m} d\nu$$

(16c)

where $\delta = \frac{p_{\text{env}} - 1}{\chi}, \xi = 1 + \frac{1}{\chi}$, and $\bar{N}_e$ is the average number of nearest neighbors of the constellation (one for BPSK and two for QPSK). Note that the approximations in (16a)–(16c) become exact for the BPSK case.

B. Perfect Fast Power Control

When the transmitter and the receiver have perfect knowledge of the channel state information, the transmitter can perfectly cancel the effect of fading by controlling the transmit signal power such that a constant desired post-MRC SNR (φ_{target}) is

achieved at the receiver. This process is referred to as the perfect fast power control algorithm.

To achieve the desired post-MRC SNR per bit, the following condition needs to be satisfied:

$$E_b = \frac{\varphi_{\text{target}}}{\gamma} \quad \text{for system A,B}$$

or

$$E_b = \frac{2\varphi_{\text{target}}}{\gamma} \quad \text{for system C.} \tag{17}$$

The average transmit energy per bit for systems A, B, and C can be calculated using a Fourier transform identity as follows:

$$E[E_b] = (2)\varphi_{\text{target}} E\left[\frac{1}{\gamma}\right] = (2)\varphi_{\text{target}} \int_{-\infty}^{0} j\Phi_\gamma(s) ds. \tag{18}$$

Closed-form expressions for the average transmit energy per bit for systems A, B, and C can be obtained by substituting the correlation matrix associated with the system and solving the integral.

1) System A

Case 1: $\Lambda_A = I_2$

$$E[E_b] = \frac{\varphi_{\text{target}} m}{\bar{\gamma}(2m-1)}. \tag{19}$$

Case 2: $\Lambda_A \neq I_2$, where the expression is shown in (20) at the bottom of the page.

2) System B

Case 1: $\Lambda_B = I_4$

$$E[E_b] = \frac{\varphi_{\text{target}} m}{\bar{\gamma}(4m-1)} \tag{21}$$

Case 2: $\Lambda_B \neq I_4$, where the expression is shown in (22) at the bottom of the page.

3) System C

Case 1: $\Lambda_C = I_4$

$$E[E_b] = \frac{\varphi_{\text{target}} m}{(\bar{\gamma}/2)(4m-1)}. \tag{23}$$

Case 2: $\Lambda_C \neq I_4$

$$E[E_b] = \begin{cases} \frac{\varphi_{\text{target}}}{(\bar{\gamma}/2)} \sum_{i=1}^{4} \frac{k_i}{\lambda_i} ln(\lambda_i), & \text{when } m=1 \\ \text{no closed-form solution,} & \text{otherwise} \end{cases} \tag{24}$$

where $K(x,y) = \prod_{i=1}^{y}(2x-2i-1);$ $\sum_{i=1}^{4} \frac{k_i}{1+x\lambda_i} = \prod_{i=1}^{4} (1+x\lambda_i)^{-1};$ $\omega = \sqrt{\xi^2 + 4\delta};$ and δ and ξ are as previously defined.

IV. ANALYTICAL RESULTS

Previously, we have presented polarization diversity as an additional dimension in lieu of, or combined with, spatial diversity. Consequently, the results that follow provide the comparative performance of polarization diversity with and without spatial diversity. Since power consumption is a very important factor in cellular systems, the required transmit power is used as the performance baseline. All systems are compared to the reference system, which is defined as a two-branch receive diversity system wherein the two receiver branches have the same average receive signal power and are uncorrelated. This system can be viewed as a perfect spatial diversity system wherein the two VPol antennas are far enough from each other that they are uncorrelated. Otherwise, it can also be viewed as a polarization diversity system where $\rho_{\text{env}} = 0$ and $\chi = 0$ dB. It is important to note that such a system is an ideal system and is unlikely to be found in a practical wireless system.

The ratio between the required transmit power of the reference system and the required transmit power of the system of interest is called the performance gain and is used to define the system performance relative to the reference system. Positive gain indicates that, relative to the reference system, the system requires less transmit power to achieve the same system performance.

A. No Power Control

Figs. 3 and 4 plot $\bar{P}_e$ versus $\bar{\varphi}$ for systems A and B with BPSK modulation in Rayleigh fading channels for specified values of ρ_{env} and χ. As expected, the best performance occurs when $\rho_{\text{env}} = 0$ and $\chi = 0$ dB. Other curves quantify the degradation in system performance as ρ_{env} and/or χ increase.

The performance gain is defined as the reduction in the required transmit power, compared to the reference system, to achieve the desired $\bar{P}_e$. It is observed from Figs. 3 and 4 that the gain increases as $\bar{P}_e$ decreases. For a desired $\bar{P}_e$ of 10^{-3} and BPSK modulation, the gain of system A and system B for Rayleigh fading channels (solid lines), and Nakagami-m fading channels with $m = 2$ (dotted lines) are shown in Figs. 5 and 6, respectively.

$$E[E_b] = \begin{cases} \frac{\varphi_{\text{target}}}{\bar{\gamma}\omega} ln\left(\frac{\xi+\omega}{\xi-\omega}\right), & \text{when } m=1 \\ \frac{\varphi_{\text{target}}}{\bar{\gamma}} \left(\frac{m\xi}{(m-1)\omega^2} + \sum_{i=1}^{m-2} \frac{m\xi(2\delta)^i (m-2-i)! K(m,i)}{(m-1)! \omega^{2i+2}} + \frac{m(2\delta)^{m-1} K(m,m-1)}{(m-1)! \omega^{2m-1}} ln\left(\frac{\xi+\omega}{\xi-\omega}\right) \right), & \text{otherwise} \end{cases} \tag{20}$$

$$E[E_b] = \frac{\varphi_{\text{target}}}{\bar{\gamma}} \left(\frac{m\xi}{(2m-1)\omega^2} + \sum_{i=1}^{2m-2} \frac{m\xi(2\delta)^i (2m-2-i)! K(2m,i)}{(2m-1)! \omega^{2i+2}} + \frac{m(2\delta)^{2m-1} K(2m,2m-1)}{(2m-1)! \omega^{4m-1}} ln\left(\frac{\xi+\omega}{\xi-\omega}\right) \right) \tag{22}$$
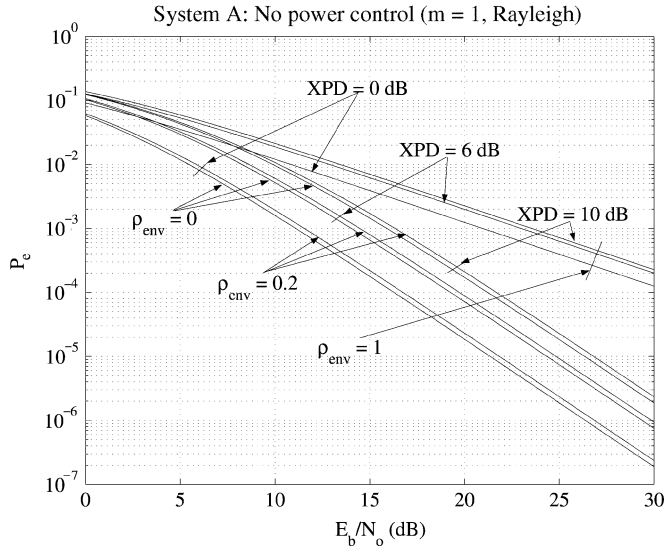
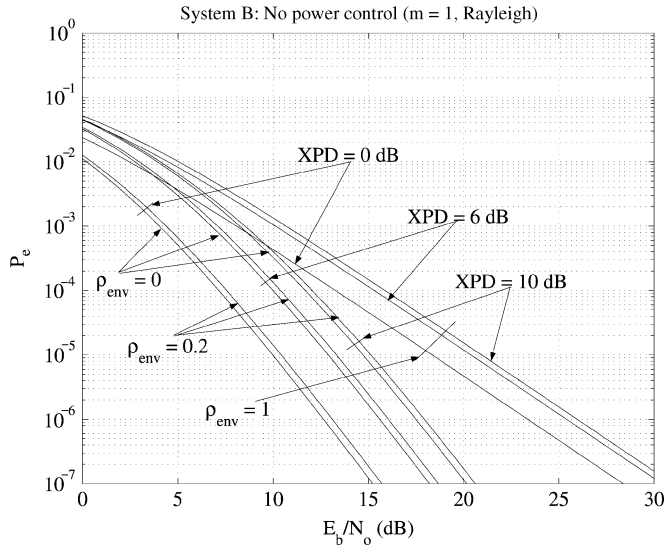Fig. 3. Average symbol error probability of system A assuming no power control and BPSK.

Fig. 4. Average symbol error probability of system B assuming no power control and BPSK.
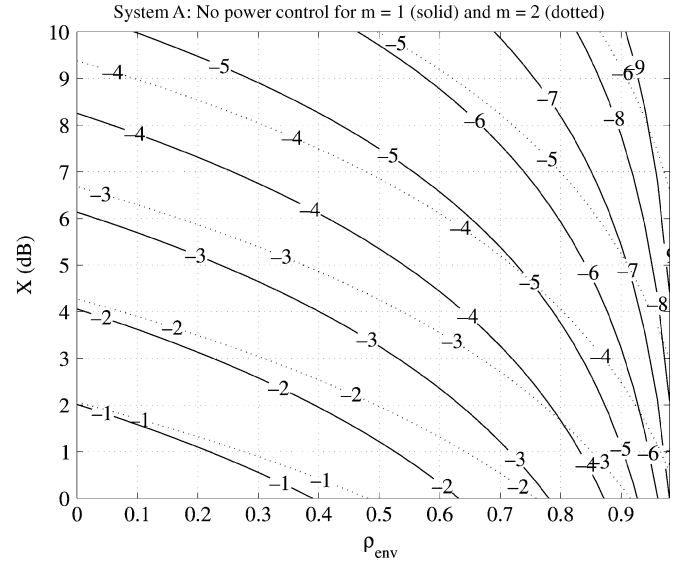

Fig. 5. Performance gain of system A compared to the reference system (no power control, BPSK).

Fig. 6. Performance gain of system B compared to the reference system (no power control, BPSK).

It can be seen from Fig. 6 that when χ is large and ρ_{env} is equal to one, the polarization diversity is no longer efficient, and the system is equivalent to a perfect two-branch space diversity system (or the reference system). The performance gain in a realistic channel can be estimated by using the measurement data from the urban environment. The data show that the envelope correlation is generally less than 0.2 and the XPD has an average of 6 dB. It can be deduced from Figs. 5 and 6 that the loss from using system A compared to the reference system is 3–3.4 dB for Rayleigh fading channels, and 2.9–3.1 dB for Nakagami-m fading channels with $m = 2$, and the gain from using system B compared to the reference system is 4–4.3 dB for Rayleigh fading channels and 2.1–2.3 dB for Nakagami-m fading channels with $m = 2$.

In order to appreciate the simplicity and the accuracy of the analysis presented in this paper, we extend (16c) to 16-QAM modulation and compare the results with the results from [11], which was derived using the Chernoff bound approach, and with our simulation results. The extended analysis uses the nearest neighbors approximation [13], and the expression for the bit error probability corresponding to 16-QAM can be expressed as
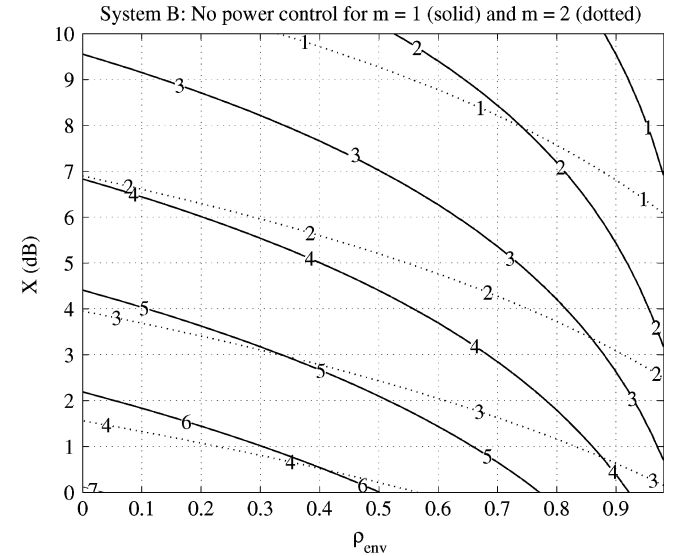
$$\bar{P}_{e,C,16\text{QAM}} \approx \frac{3}{\pi} \int_0^{\frac{\pi}{2}} \prod_{i=1}^{4} \left(1 + \frac{\tilde{\gamma}\lambda_i}{10 \cdot 2\sin^2 \nu} \right)^{-1} d\nu \quad (25)$$

where $\tilde{\gamma}$ is the SNR as defined in [11], three is the number of the average nearest neighbors, and ten is the scaling factor used to maintain the same average transmit power between the QPSK and 16-QAM.

The comparison between (25), the result from [11], and the simulation result when $\sqrt{t_1} = \sqrt{t_2} = 0.7$, $\sqrt{r_1} = \sqrt{r_2} = 0.1$, $\chi_1 = \chi_2 = 5$, and $\delta = 1$ is shown in Fig. 7. It is clear that
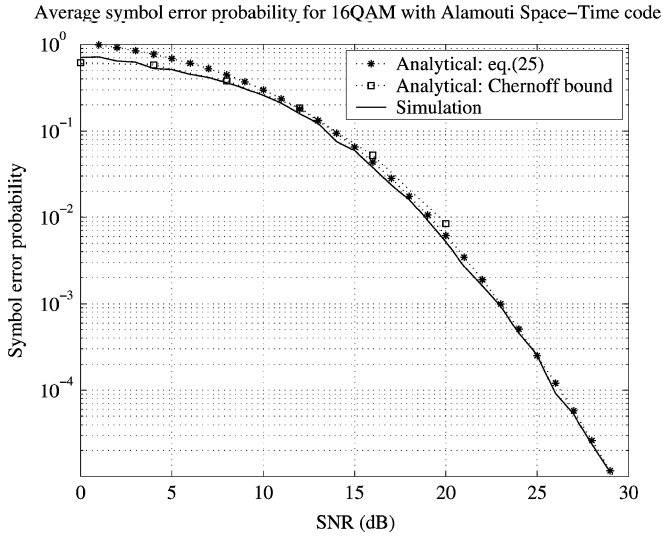
Average symbol error probability for 16QAM with Alamouti Space−Time code

Fig. 7. Comparison between the simulation result, the analytical result from [11] and the analytical result from (25) for Rayleigh fading channels.
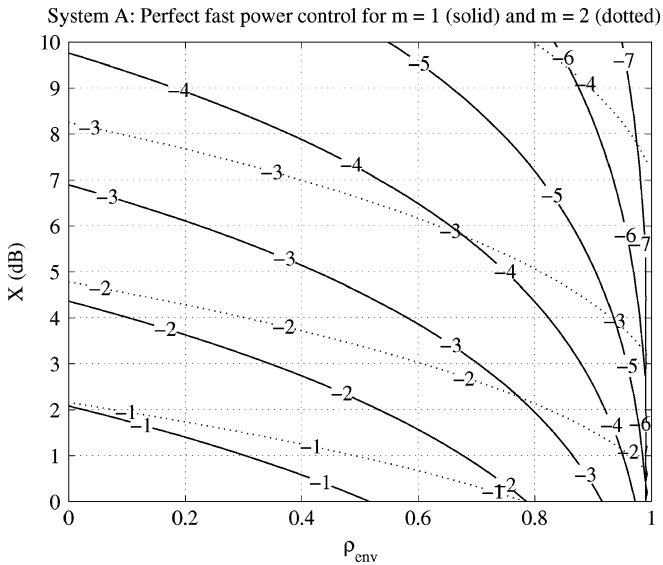
System A: Perfect fast power control for m = 1 (solid) and m = 2 (dotted)

Fig. 8. Performance gain of system A compared to the reference system (perfect fast power control).

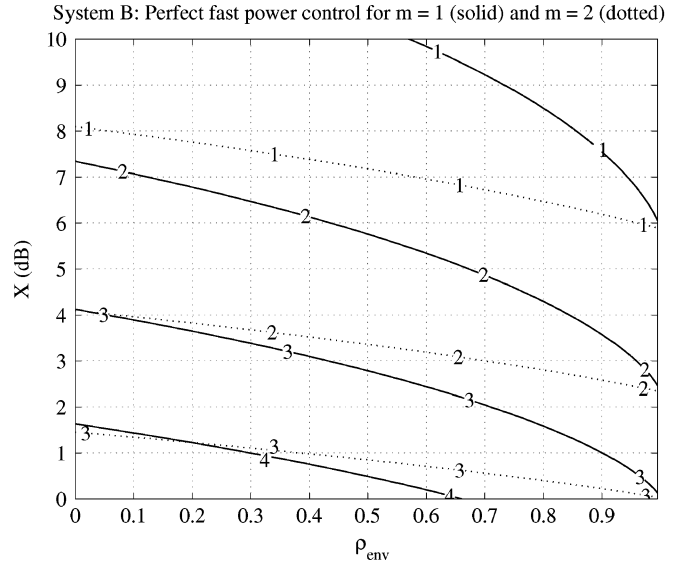System B: Perfect fast power control for m = 1 (solid) and m = 2 (dotted)

Fig. 9. Performance gain of system B compared to the reference system (perfect fast power control).

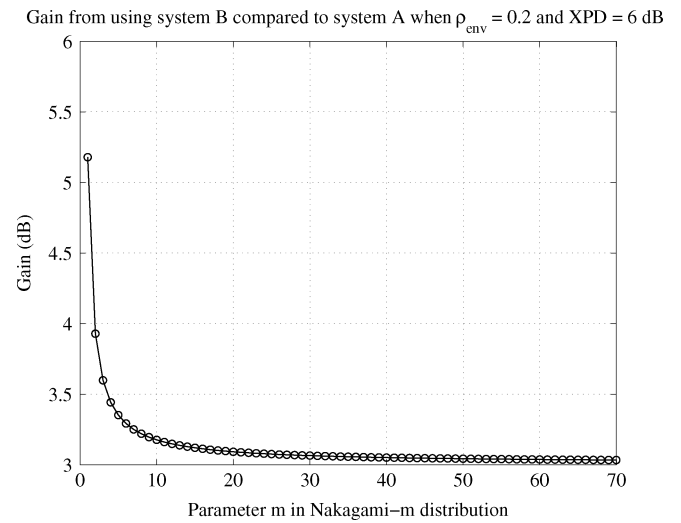Gain from using system B compared to system A when ρ_{env} = 0.2 and XPD = 6 dB

Fig. 10. Gain from using system B compared to system A when $\rho_{env} = 0.2$ and $\chi = 6$ dB as a function of m (Nakagami-m distribution parameter).

(25) accurately predicts the system performance at high SNR. However, as a result of the nearest neighbors approximation, the prediction is not accurate at low SNR.

B. Perfect Fast Power Control

The performance gain in the case of perfect fast power control is defined as the reduction in the required transmit power to achieve the desired post-MRC SNR compared to the reference system. Figs. 8 and 9 show the gain of system A and system B in Rayleigh fading channels (solid lines), and Nakagami-m fading channels with $m = 2$ (dotted lines), as a function of ρ_{env} and χ, respectively. The performance in a realistic urban environment can be approximated using the values of ρ_{env} and χ measured from the actual channel. With ρ_{env} less than 0.2 and the average χ of 6 dB, system A experiences a loss of 2.6–3 dB for Rayleigh

fading channels and a loss of 2.3–2.5 dB for Nakagami-m fading channels with $m = 2$, while system B experiences a gain of 2.2–2.4 dB for Rayleigh fading channels and a gain of 1.4–1.5 dB.

The value of m in Nakagami-m distribution determines the severity of fading. The smaller m is, the more severe the fading condition is. Fig. 10 shows the performance gain of system B compared to system A when ρ_{env} is 0.2 and χ is 6 dB. The channel approaches an AWGN channel when m approaches infinity, and we can see from Fig. 10 that the gain approaches 3 dB, which represents the gain from doubling the number of antennas in an AWGN channel, as expected.

Unlike systems A and B, system C is a function of more parameters, and a simple contour plot similar to Figs. 8 and 9 does not exist. We have chosen a simple channel characteristic where $\chi_1 = \chi_2, t_1 = t_2 = 0.2$, and $r_1 = r_2$ as an example to illustrate
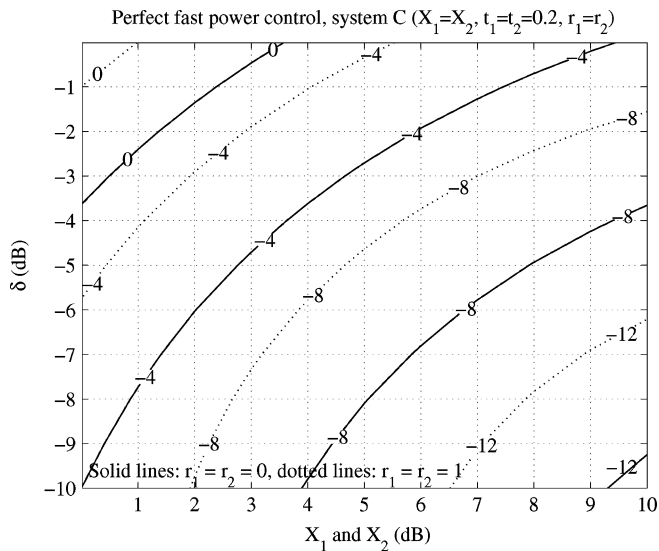
Fig. 11. Performance gain of system C for the sample channel compared to the reference system (perfect fast power control, Rayleigh).

the effect of the channel characteristic on system performance. Fig. 11 shows the gain of system C under this particular channel characteristic. The 0-dB line determines the channel condition where system C performs as well as the reference system, and the area on the left side of the 0 dB line represents the scenario wherein system C outperforms the reference system. It is interesting to point out that even though system C needs only slightly more space than a SISO system, under this particular channel characteristic, this compact system can achieve similar (or even better) performance compared to the perfect two-branch receive diversity system by use of space-time code and polarization receive diversity. We can also see from Fig. 11 that as r_1, r_2 increases (the channel gets worse), the 0-dB line moves to the left, and the area where system C outperforms the reference system gets smaller.

V. CONCLUSION

It has been shown that polarization diversity systems can provide significant performance enhancements either in lieu of, or in combination with, spatial diversity systems, despite the inherent power imbalance between polarizations. We have derived the relationship between the polarization characteristic, which is represented by the envelope correlation and the power imbalance, and the system performance in correlated Nakagami-m fading channels with the MRC diversity receiver. More specifically, the average symbol error probability as a function of SNR and the polarization characteristic (assuming no power control), and the average transmit power as a function of post-MRC SNR and the polarization characteristic (assuming perfect fast power control), are derived.

We have shown that the performance of polarization diversity in a realistic channel can easily be obtained by substituting the envelope correlation and the cross-polarization discrimination measured from the actual channel into the analytical expressions provided. The power imbalance does limit system performance,

as expected. Nevertheless, it is shown that the gain achieved with polarization diversity can be significant. The advantage of polarization diversity ultimately depends on the particular channel characteristic.

It has also been shown that the analysis can easily be extended to a more complex system. The extension of system C to 16-QAM with the nearest neighbors approximation has been shown to match the simulation result, especially at high SNR.

REFERENCES

[1] R. Visoz and E. Bejjani, "Matched filter bound for multichannel diversity over frequency-selective Rayleigh-fading mobile channels," *IEEE Trans. Veh. Technol.*, vol. 49, no. 5, pp. 1832–1845, Sep. 2000.

[2] R. G. Vaughan, "Polarization diversity in mobile communications," *IEEE Trans. Veh. Technol.*, vol. 39, no. 3, pp. 177–186, Aug. 1990.

[3] A. M. D. Turkmani, A. A. Arowojolu, P. A. Jefford, and C. J. Kellett, "An experimental evaluation of the performance of two-branch space and polarization diversity schemes at 1800 MHz," *IEEE Trans. Veh. Technol.*, vol. 44, no. 3, pp. 318–326, May 1995.

[4] F. Lotse, J.-E. Berg, U. Forssen, and P. Idahl, "Base station polarization diversity reception in macrocellular systems at 1800 MHz," in *Proc. IEEE Vehicular Technology Conf.*, Atlanta, GA, 1996, pp. 1643–1646.

[5] W. C. Y. Lee and Y. S. Yeh, "Polarization diversity system for mobile radio," *IEEE Trans. Commun.*, vol. COM-26, pp. 912–923, Oct. 1972.

[6] T. Neubauer and P. C. F. Eggers, "Simultaneous characterization of polarization matrix components in pico cells," in *Proc. IEEE Vehicular Technology Conf.*, vol. 3, Amsterdam, The Netherlands, 1999, pp. 1361–1365.

[7] J. Jootar and J. R. Zeidler, "Performance analysis of polarization receive diversity in correlated Rayleigh fading channels," in *Proc. IEEE Globecom'03 Conf.*, San Francisco, CA, Dec. 2003, pp. 774–778.

[8] M. Nakagami, "The m-distribution, a general formula of intensity distribution of rapid fading," in *Statistical Methods in Radio Wave Propagation*, W. G. Hoffmann, Ed. New York: Pergamon, 1960.

[9] J. Luo, J. R. Zeidler, and S. McLaughlin, "Performance analysis of compact antenna arrays with MRC in correlated Nakagami fading channels," *IEEE Trans. Veh. Technol.*, vol. 50, no. 1, pp. 267–277, Jan. 2001.

[10] S. M. Alamouti, "A simple transmit diversity technique for wireless communications," *IEEE J. Sel. Areas Commun.*, vol. 16, no. 10, pp. 1451–1458, Oct. 1998.

[11] R. Nabar, H. Bolcskei, V. Erceg, D. Gesbert, and A. J. Paulraj, "Performance of multiantenna signaling techniques in the presence of polarization diversity," *IEEE Trans. Signal Process.*, vol. 50, no. 10, pp. 2553–2562, Oct. 2002.

[12] M. Schwartz, W. R. Bennet, and S. Stein, *Communication Systems and Techniques*. New York: McGraw-Hill, 1966.

[13] J. M. Cioffi, *Class reader for EE379A-Digital Communication: Signal Processing*. Stanford, CA: Stanford Univ, Jan. 2005.
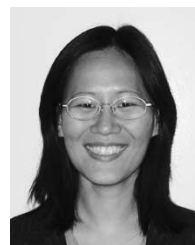
Jittra Jootar (S'02) received the B.S. degree in electrical engineering from Chulalongkorn University, Bangkok, Thailand, in 1997 and the M.S. degree in electrical engineering from Stanford University, Stanford, CA, in 1999. Since 2002, she has been working toward the Ph.D. degree at the Department of Electrical and Computer Engineering, University of California at San Diego, La Jolla.

From 1999 to 2002, she was with QUALCOMM Inc., San Diego, CA, where she worked on Bluetooth and WCDMA development. Her research interests include modulation and coding for mobile communication systems.

Jean-Francois Diouris (M'92) received the Ph.D. degree in electrical engineering from the University of Rennes I, Rennes, France, in 1991.

From 1992 to 1999, he was an Assistant Professor with IRESTE, University of Nantes, Nantes, France. He is currently a Professor with Polytech'Nantes, University of Nantes. His current research interests include digital communications, antenna processing, and software radio.

James R. Zeidler (M'76–SM'84–F'94) is a research scientist/senior lecturer in the Department of Electrical Engineering, University of California at San Diego (UCSD), La Jolla. He is a faculty member of the UCSD Center for Wireless Communications and the University of California Institute for Telecommunications and Information Technology. He has more than 200 technical punlications and 13 patents for communication, signal processing, data compression techniques, and electronic devices.

Dr. Zeidler was elected Fellow of the IEEE in 1994 for his technical contributions to adaptive signal processing and its applications.

He received a Frederick Ellersick award from the IEEE Communications Society at the IEEE Military Communications Conference in 1995, the Navy Meritorious Civilian Service Award in 1991, and the Lauritsen–Bennett Award for Achievement in Science from the Space and Naval Warfare Systems Center in 2000. He was an Associate Editor of the IEEE TRANSACTIONS ON SIGNAL PROCESSING and a member of the technical committee on Underwater Acoustic Signal Processing for the IEEE Signal Processing Society.